


RESEARCH

Open Access



Inhibition of circALPK2 enhances proliferation and therapeutic potential of human pluripotent stem cell-derived cardiomyocytes in myocardial infarction

Hongchun Wu^{1†}, Xue Jiang^{1†}, Hao Fan^{1†}, Jingjing Li¹, Yuan Li¹, Yingjiong Lin¹, Dandan Zhao¹, Xinglong Han¹, Miao Yu¹, Jun-Ming Tang², Shijun Hu^{1*}  and Wei Lei^{1*}

Abstract

Background Understanding the mechanisms regulating human cardiomyocyte proliferation holds significant promise for developing effective therapies to enhance cardiac regeneration and repair. This study investigates the role of *circALPK2*, a circular RNA derived from the back-splicing of the 4th exon of alpha protein kinase 2 (*ALPK2*), in regulating cardiomyocyte proliferation and its therapeutic efficacy in myocardial infarction (MI) treatment.

Methods Human embryonic stem cell-derived cardiomyocytes (hESC-CMs) were used to assess the expression and function of *circALPK2*. Lentiviral shRNA-mediated knockdown of *circALPK2* was performed in hESC-CMs, followed by RNA sequencing to identify targeted genes and biological processes. The proliferative capacity of wild-type and *circALPK2* knockdown hESC-CMs was evaluated using CCK-8 assay, EdU staining and RT-qPCR analysis of cell cycle-related genes. Dual luciferase assays were conducted to validate the predicted miRNA targets and their downstream effects. For in vivo evaluation, MI mice were injected with either wild-type or *circALPK2* knockdown hESC-CMs, and the therapeutic potential was assessed by echocardiographic and histological analyses.

Results We identified *circALPK2* as a negative regulator of cell proliferation in hESC-CMs. *CircALPK2* was abundantly expressed in hESC-CMs. Knockdown of *circALPK2* significantly enhanced cell proliferation in hESC-CMs, as demonstrated by CCK-8 assays ($p < 0.001$) and EdU staining ($p < 0.001$), and accelerated the expression of cell cycle-related genes, including *CCNA2* ($p < 0.05$) and *CDK1* ($p < 0.01$). Furthermore, *circALPK2* was found to function as a sponge to inhibit *miR-9* activity, while *miR-9* mimics significantly boosted the proliferative capacity of hESC-CMs. Glycogen synthase kinase 3 β (*GSK3B*), a key inhibitor of WNT signaling, was identified as a direct target of *miR-9*, mediating the regulation of cardiomyocyte proliferation. Importantly, *circALPK2* knockdown improved the myocardial

[†]Hongchun Wu, Xue Jiang and Hao Fan contributed equally to this work.

*Correspondence:
Shijun Hu
shijunhu@suda.edu.cn
Wei Lei
leiwei@suda.edu.cn

Full list of author information is available at the end of the article



© The Author(s) 2025. **Open Access** This article is licensed under a Creative Commons Attribution-NonCommercial-NoDerivatives 4.0 International License, which permits any non-commercial use, sharing, distribution and reproduction in any medium or format, as long as you give appropriate credit to the original author(s) and the source, provide a link to the Creative Commons licence, and indicate if you modified the licensed material. You do not have permission under this licence to share adapted material derived from this article or parts of it. The images or other third party material in this article are included in the article's Creative Commons licence, unless indicated otherwise in a credit line to the material. If material is not included in the article's Creative Commons licence and your intended use is not permitted by statutory regulation or exceeds the permitted use, you will need to obtain permission directly from the copyright holder. To view a copy of this licence, visit <http://creativecommons.org/licenses/by-nc-nd/4.0/>.

repair potential of hESC-CMs when injected into infarcted mouse hearts, as indicated by improved left ventricular ejection fraction ($p < 0.01$) and fractional shortening ($p < 0.05$).

Conclusions Our study identifies the *circALPK2/miR-9/GSK3B* axis as a novel target for promoting cardiomyocyte proliferation and enhancing cardiac regeneration.

Keywords Cardiomyocyte proliferation, *circALPK2*, *miR-9*, *GSK3B*, Myocardial infarction

Introduction

The inability of adult cardiomyocytes to renew after cardiac injury is a key cause of the high mortality of cardiovascular diseases (CVDs), which contributed to 19.05 million deaths globally in 2020 [1]. Therefore, myocardial regeneration in patients with cardiac injury is a long-sought goal in the clinical treatment of CVDs. Boosting of endogenous cardiomyocyte proliferation and transplantation of exogenous cardiomyocytes have now emerged as two appealing approaches for cardiac repair and regeneration [2, 3]. While the regenerative potential has been uncovered in mammalian newborn hearts, understanding mechanisms controlling postnatal cardiomyocyte proliferation will indisputably promote the identification of novel targets for stimulating adult cardiac regeneration [4, 5]. Human pluripotent stem cell-derived cardiomyocytes (hPSC-CMs) represent a promising cell source for both modeling human embryonic and postnatal cardiomyocytes and developing stem cell-based regenerative therapy. Meanwhile, investigating the regulation of proliferation in hPSC-CMs will help to improve the scalability of hPSC-CM production to meet the demands of pre-clinical and clinical studies, and address low survival and engraftment rate of transplanted cells, a major hurdle for the clinical application [6].

Non-coding RNAs (ncRNAs), particularly microRNAs (miRNAs), circular RNAs (circRNAs), and long ncRNAs, emerged as critical regulators of cardiomyocyte proliferation during heart development and cardiac regeneration [7]. Numerous miRNAs, such as *miR-25*, *miR-199a*, *miR-204*, *miR-210*, *miR-515*, *miR-519e*, and *miR-590*, have been shown to promote cardiomyocyte proliferation via the regulation of mRNA stability and translation [8–12]. *In contrast, relatively fewer studies have explored the roles of circRNAs in regulating cardiomyocyte proliferation* [13–15]. Mechanistically, circRNAs can act as miRNA sponges and scaffolds for RNA-binding proteins [16]. For example, circRNA *Nfix* was found to reduce cardiomyocyte proliferation through binding to transcription factor Ybx1 and mediating its degradation, and meanwhile inhibit angiogenesis via sponging *miR-214* to promote *Gsk3b* (glycogen synthase kinase 3 β) expression and repress β -catenin activity [13]. Despite the encouraging evidences, circRNA research, particularly in cardiac regeneration and repair, is still in its infancy.

In a previous study, we revealed a dynamic expression of circRNAs during cardiac differentiation from hPSCs, including a circRNA (*circALPK2*) formed by circulation of the 4th exon of alpha protein kinase 2 (*ALPK2*) [17]. As a negative regulator of WNT signaling, *ALPK2* depletion led to defective cardiogenesis in zebrafish and hPSCs [18]. However, *Alpk2*-knockout mice exhibited normal cardiac morphology and function [19]. Further studies are needed to address the rationale for the phenotypic differences between species. Given its specific expression in the human heart and hPSC-derived cardiomyocytes, we speculate *circALPK2* might also be involved in human cardiogenesis, which would further complicate the regulatory network.

In the current study, by using human embryonic stem cell-derived cardiomyocytes (hESC-CMs) and myocardial infarction mice models, we demonstrated that *circALPK2* is a negative regulator of cardiomyocyte proliferation and myocardial repair. Mechanistically, *circALPK2* can serve as a sponge of *miR-9* to relieve its inhibitory effect on the expression of *GSK3B*, ultimately inhibiting the WNT signaling pathway that is crucial for cardiomyocyte proliferation. Finally, the knockdown of *circALPK2* enhances the myocardial repair capacity of hESC-CMs when injected into the infarcted mouse heart.

Methods

Cell culture

Experiments involving human cells were approved by the Ethics Committee of First Affiliated Hospital of Soochow University (No. 2022–519). The H1 human embryonic stem cells (hESCs, WiCell Research Institute, USA) were routinely maintained in PSCeasy medium (Cellapy, China) on Matrigel-coated plates (Corning, USA), and were passaged with 0.5 mM EDTA at 80% confluence [20]. Dissociation-induced cell apoptosis was prevented by supplementing with 2 μ M Thiazovivin (Selleck Chemicals, USA) in the culture medium for 24 h. HEK293T cells were cultured in high-glucose DMEM (4.5 g/L D-Glucose, Thermo Fisher, USA) supplemented with 10% (vol/vol) fetal bovine serum (Biological Industries, USA), 100 μ g/mL streptomycin and 100 U/mL penicillin (Thermo Fisher, USA). All cells were maintained within a humidified 37 $^{\circ}$ C/5% CO₂ cell culture incubator.

Cardiomyocyte differentiation from hESCs

Differentiation of hESCs into cardiomyocytes was conducted following a previously described protocol [21]. When hESCs reached 90% confluence, the culture medium was replaced with cardiac differentiation medium (CDM3) consisting of RPMI 1640 medium (Thermo Fisher, USA), recombinant human albumin (Sigma-Aldrich, USA), and L-ascorbic acid 2-phosphate (Sigma-Aldrich, USA). Meanwhile, cells were successively treated with 4 μ M CHIR99021 (Sigma-Aldrich, USA) for 2 days and 2 μ M Wnt-C59 (Selleck Chemicals, USA) for another 2 days. Cells were maintained in CDM3 from day 5 onwards, and spontaneous beating was observed at about day 9. The hESC-CMs were metabolically purified by 4-day culture in glucose-free RPMI 1640 (Thermo Fisher, USA) supplemented with 5 mM sodium DL-lactate (Sigma-Aldrich, USA).

Lentiviral shRNA knockdown of *circALPK2*

The shRNA fragment specifically targeting the back-splice junction site of *circALPK2* was synthesized by GENEWIZ (China), and was cloned into the MluI/ClaI sites of the pLVTHM vector (Addgene, USA). The newly developed vector was then transfected into HEK293T cells, along with the helper plasmids psPAX2 and pMD2.G, for virus packaging. After concentrated from the cell culture medium, the control and *circALPK2* shRNA lentiviral particles were used to infect hESC-CMs for 48 h, so as to induce knockdown of *circALPK2* in hESC-CMs.

Lentiviral overexpression of *GSK3B*

The coding sequence region of *GSK3B* was amplified from the cDNAs by using the KOD-Plus-Neo (TOYOBO, Japan). The PCR fragment was inserted into the EcoRI/BamHI sites in the pCDH-CMV-MCS-EF1-copGFP vector (SBI, USA) to generate the lentiviral expression vector for *GSK3B*. The control and *GSK3B*-overexpressing vectors were then packaged and transfected into hESC-CMs, as mentioned above.

RNA sequencing and bioinformatics analysis

In brief, hESC-CMs subjected to lentivirus-mediated knockdown of *circALPK2* or its negative control were collected for total RNA extraction. The cDNA library was constructed using a TruSeq RNA Sample Prep Kit and sequenced on the HiSeq2000 platform (Novogene, China). Sequence reads were mapped to the reference genome using HISAT2. Bowtie2 was applied to align the clean reads to the reference coding gene set. EdgeR was applied to identify DEGs between samples. Gene Ontology (GO) term enrichment and Kyoto Encyclopedia of Genes and Genomes (KEGG) pathway analysis were

performed using the OmicShare tools, a free online platform for data analysis (<https://www.omicshare.com/tools>).

RT-PCR and RT-qPCR

Total RNAs were extracted from the cells using Trizol Reagent (Sigma-Aldrich, USA). A total of 500 ng RNAs were subjected to reverse transcription using a PrimeScript reverse transcriptase reagent kit (TaKaRa, Japan), followed by regular PCR (RT-PCR) detection with the PCR Amplification Kit (TaKaRa, Japan) or quantitative real-time PCR (RT-qPCR) detection with the SYBR Premix Ex Taq kit (TaKaRa, Japan). The PCR for *circALPK2* was performed using divergent primers to amplify only circular transcripts, and the products were further confirmed by Sanger sequencing. For miRNA detection, the specific stem-loop primers for each miRNA were utilized in a cDNA synthesis reaction. Primers used in this study are listed in Supplementary Table 1.

EdU staining

The hESC-CMs were cultured in the 35-mm cell culture dishes for 3 days, and subsequently incubated with 10 μ M EdU in the cell culture medium at 37 °C for 4 h. EdU that was incorporated into newly synthesized DNA was then labeled with the Cell-Light EdU Apollo® 567 In Vitro Kit (Ribobio, China) according to the manufacturer's instructions. The cells were then subjected to successive incubation with 5% BSA in PBS at room temperature for 1 h, the Cardiac Troponin T antibody (15513-1-AP, Proteintech, USA) at 4 °C overnight, and the corresponding fluorescent secondary antibody (Jackson ImmunoResearch, USA) at room temperature for 1 h. Nuclei were stained with Hoechst 33,342 for 15 min. Images were acquired with an LSM880 Zeiss confocal laser scanning microscope (Carl Zeiss, Germany). EdU-positive cells were calculated from the images using ImageJ software.

Dual luciferase assay

We conducted four luciferase reporter vectors in this study, carrying the *circALPK2* sponge sites for *miR-9-5p*, wild-type *GSK3B* 3'-UTR, and their corresponding fragments with mutant *miR-9-5p* binding sites, respectively. The DNA fragments were synthesized by GENEWIZ (China), and then inserted into the SacI/XhoI sites of the pGL3-control vector (Promega, USA), immediate downstream of the firefly luciferase gene. The reporter vectors carrying wild-type or mutant fragments were transfected into HEK293T cells, along with *miR-9-5p* mimics (Ribobio, China), using a Lipofectamine® 3000 Transfection Reagent (Thermo Fisher, USA). The Renilla luciferase reporter vector pRL-TK (Promega, USA) was co-transfected into HEK293T cells as an internal reference. After 48 h of transfection, the cells were lysed and analyzed for

luciferase activity using the Dual-Luciferase Reporter Assay System (Promega, USA) according to the manufacturer's instructions.

CCK-8 assay

The hESC-CMs were replated on the 96-well plate at 30,000 cells/well and cultured for 24 h, followed by incubation with 10% CCK-8 solution (Beyotime, Suzhou, China) in the culture medium for 4 h. OD values under 450 nm were measured by a microplate reader (Biotek, USA).

Animal studies

Surgical procedures and animal care protocols in this study were approved by the Ethics Committee of the First Affiliated Hospital of Soochow University (No. 2022–519). The work has been reported in line with the ARRIVE guidelines 2.0. Healthy severe combined immune deficiency (SCID/beige) female mice were purchased from the Animal Center of Soochow University (Suzhou, China), and maintained under the same specific pathogen-free conditions. Female mice (8 weeks old) were used in this study due to their better survival rates following myocardial infarction and to eliminate gender influence on heart function. A total of 28 mice were randomly divided into four groups ($n=7$ for each group), including the sham-operated group (Sham), the myocardial infarction group (MI), the MI plus wild-type hESC-CM injection group (MI+CMs) and MI plus *circALPK2*-knockdown hESC-CM injection group (MI+sh-*circALPK2*-CMs). Myocardial infarction was introduced to mice under isoflurane anesthesia (4% induction, 1.5% maintenance) through ligation of the mid-left anterior descending artery (LAD) by an experienced microsurgeon who was blinded to the group assignments. For the latter two groups, 1×10^6 wild-type or *circALPK2*-knockdown hESC-CMs in PBS were injected into three sites beneath the ligation position immediately after LAD surgery. An equal volume of PBS was injected at similar positions of the infarcted mouse hearts in the MI group. The decision to perform cell injection immediately after LAD surgery was made to avoid the high mortality associated with a second thoracotomy. Post surgery, mice were recovered on the heating pad. No mice exhibited signs of pain, distress, or agitation during or after surgery, and all were included in subsequent cardiac function assessment.

Transthoracic echocardiographic analysis was performed at day 14 and day 28 post-MI using the Visual Sonics Vevo2100 system equipped with a medium frequency (30 MHz) MS-400 transducer. An investigator blinded to group designation ($n=7$ for each group). The left ventricular ejection fraction (EF) and fractional shortening (FS) were calculated using Visual Sonic

analysis software. Additionally, mice were euthanized by cervical dislocation at day 28 post-MI, and hearts from each group were harvested for assessing the area of heart fibrosis ($n=3$ for each group) and the expression of fibrotic markers ($n=3$ for each group).

Assessing cell retention post-transplantation

Cardiomyocytes differentiated from the hESC line carrying a luciferase reporter were transfected with either control or *circALPK2* shRNA lentiviral particles. The transfected cells were then injected into three sites beneath the ligation position immediately following LAD surgery in mice. For in vivo bioluminescence imaging (BLI), mice were anesthetized and administered an intraperitoneal injection of D-luciferin at 150 mg/kg (luciferin/body weight) at days 1, 3, 7, 14 and 28 post-cell transplantation, followed by image capture for 10 min with 1-min acquisition intervals. Bioluminescence data from a fixed region of interest was processed with the IVIS imaging system (PerkinElmer, USA). Cell retention and survival were quantified in units of photons per second per centimeter squared per steradian (p/s/cm²/sr) ($n=3$ for each group). For in vitro detection of the injected cells, mice were euthanized by cervical dislocation at day 7. The hearts from each group were harvested for immunofluorescence staining using an antibody specific to human cTnT.

Statistical analysis

All experimental analyses were performed at least three times. The data were analyzed using GraphPad Prism version 8.0, and presented as mean \pm SEM. Student's t-test was used for comparison between the two groups. Multiple comparisons were performed using one-way analysis of variance (ANOVA) followed by the Bonferroni post hoc test. P values < 0.05 was considered statistically significant.

Results

Enriched expression of *circALPK2* in human cardiomyocytes

Our previous study has revealed a heart-specific expression of *circALPK2*, formed by back-splicing of the 3'-end to 5'-end of the 4th exon of the *ALPK2* gene (Fig. 1A) [17]. Given the critical role of its host gene *ALPK2* in human cardiogenesis, we attempted to investigate the potential effect of *circALPK2* in human cardiomyocytes.

Human cardiomyocytes used in the current study were derived from hESCs via modulating WNT signaling in cardiac differentiation medium. After metabolic purification, hESC-CMs were used in subsequent experiments. The expression of *circALPK2* in hESC-CMs was verified by PCR amplification of its back-splicing region with a pair of divergent primers. While both cDNA and genomic DNA fragments could be amplified by using the

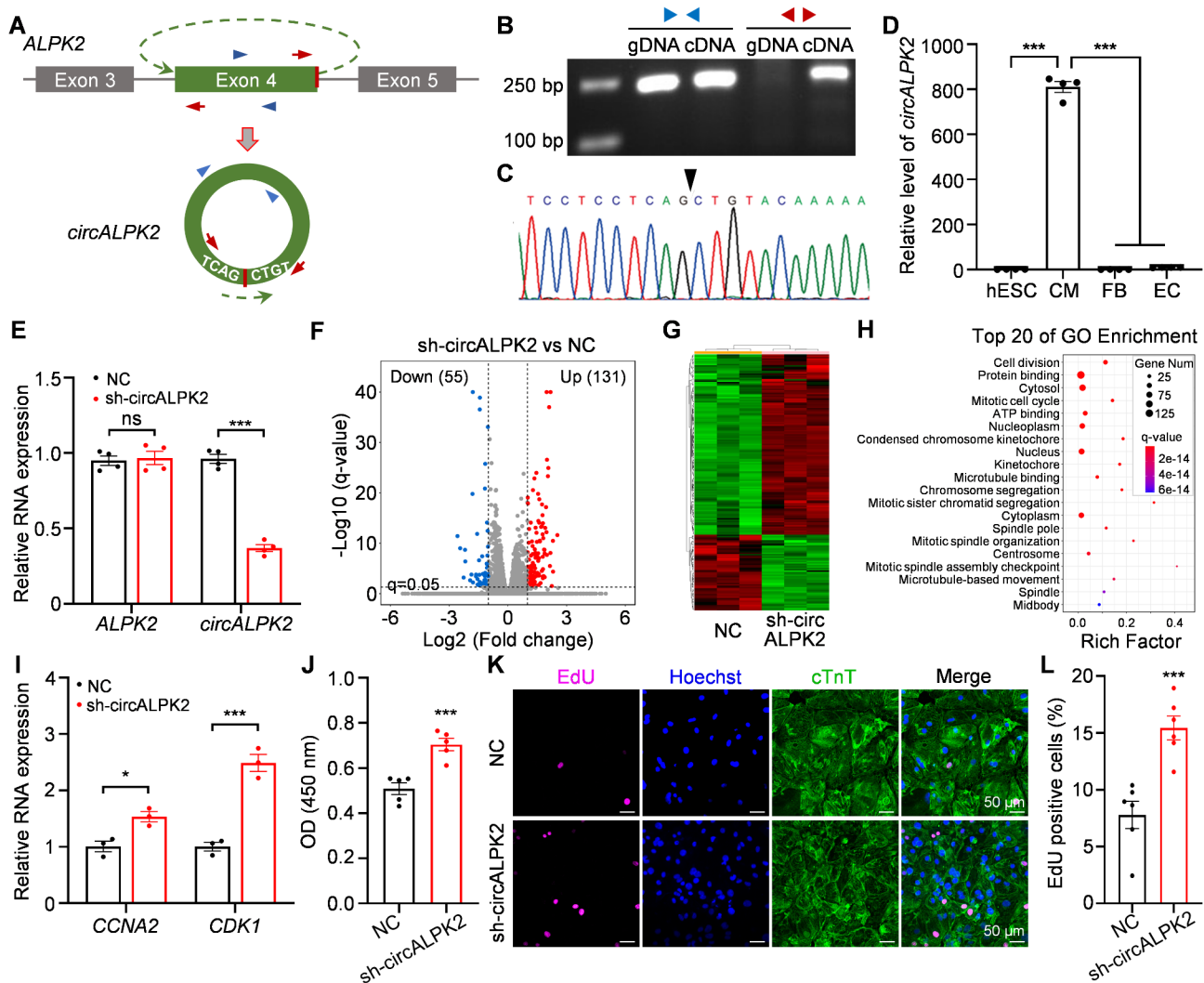


Fig. 1 Anti-proliferative effect of *circALPK2* in hESC-derived cardiomyocytes. **(A)** Schematic depiction of *circALPK2* generation by back-splicing of the 4th exon of *ALPK2*. **(B)** Representative electrophoretogram of PCR products amplified from genomic DNA (gDNA) and cDNAs with either convergent (blue arrows) or divergent (red arrows) primers. The full-length gel of the representative electrophoretogram is presented in Supplementary Figure S2. **(C)** Sanger sequencing peak map showing successful amplification of back-splicing site (dark triangle) of *circALPK2*. **(D)** RT-qPCR detection of *circALPK2* in hESCs, hESC-derived cardiomyocytes (CM), fibroblasts (FB), and endothelial cells (EC) ($n=4$). **(E)** RT-qPCR detection of linear *ALPK2* and *circALPK2* in hESC-CMs transfected with negative control (NC) and shRNAs specifically targeting *circALPK2* (sh-*circALPK2*) ($n=4$). The transfection efficiency of lentiviral shRNA vectors is presented in Supplementary Figure S3. **(F)** Volcano map showing differentially expressed genes in the control and *circALPK2* shRNA-transfected hESC-CMs ($n=3$). **(G)** Heatmap for the 186 differentially-expressed genes (DEGs) between the control and *circALPK2*-depleted hESC-CMs. **(H)** Scatter plot showing the top 20 Gene Ontology (GO) terms enriched by the DEGs with the lowest q-value. **(I)** RT-qPCR detection of cell cycle genes *CCNA2* and *CDK1* in the control and *circALPK2*-depleted hESC-CMs ($n=3$). **(J)** CCK-8 assay on cell proliferation in hESC-CMs. The OD 450 nm value is proportional to the number of viable cells in the sample ($n=5$). **(K)** Immunofluorescence images showing EdU-positive cells (magenta) in hESC-CMs (cTnT-positive, green). Nuclei were stained with Hoechst 33,342 (blue). Scale bar indicates 50 μ m. **(L)** Statistical analysis of the ratio of EdU-positive cells in control and *circALPK2*-depleted hESC-CMs ($n=6$). Data were shown as mean \pm SEM. One-way ANOVA for multiple comparisons & Student's t-test for comparisons between two groups; * $p < 0.05$, *** $p < 0.001$; ns, not significant

convergent primers, the divergent primers targeting the 4th exon resulted in a single amplicon with expected size in only cDNA but not genomic DNA samples (Fig. 1B). Furthermore, Sanger sequencing analysis confirmed that the single amplicon contained a back-splicing junction of the 4th exon of linear *ALPK2* gene (Fig. 1C). These data verified the existence of *circALPK2* in hESC-CMs.

We subsequently assessed the expression of *circALPK2* and its linear counterpart in different cardiac component cells, including hESC-CMs, fibroblasts, and endothelial cells. Unlike the linear *ALPK2* showing abundant expression in both hESC-CMs and fibroblasts (Supplementary Fig. S1A), the expression of *circALPK2* was specifically elevated in hESC-CMs (Fig. 1D). Interestingly, a significant increase of *circALPK2* expression in hESC-derived

cells was observed on day 4 of cardiac differentiation, corresponding to the cardiac progenitor cell stage (Supplementary Fig. S1B). The abundance of *circALPK2* continuously rises in hESC-CMs throughout cardiac differentiation from days 0 to 9, and remains elevated during the culture period from days 9 to 30 (Supplementary Fig. S1B), a stage during which hESC-CMs gradually lose their proliferative capacity and become more mature. The linear *ALPK2* mRNAs showed a similar expression trend with *circALPK2* during cardiac differentiation (Supplementary Fig. S1C). Although *ALPK2* is involved in cardiogenesis, the role of *circALPK2* in cardiomyocytes is still unclear.

Anti-proliferative effect of *circALPK2* in human cardiomyocytes

In order to uncover its biological functions, *circALPK2* was knocked down in hESC-CMs by lentiviral shRNAs directly targeting its back-splice junction without affecting its linear counterpart *ALPK2* (Fig. 1E). We first profiled the gene expression signatures of control and *circALPK2*-depleted hESC-CMs and identified 186 genes (fold change > 2, *p*adj < 0.05) showing significantly differential expression (Fig. 1F and G, Supplementary Table 2). GO (gene ontology) analysis showed that the significantly enriched biological processes include cell division and mitotic cell cycle (Fig. 1H). Consistently, RT-qPCR data showed significantly decreased expression of cell cycle-related genes such as *CCNA2* and *CDK1* in *circALPK2*-defective hESC-CMs (Fig. 1I). Thus, we hypothesized that *circALPK2* was associated with cardiomyocyte proliferation.

We next analyzed the proliferative capacity of hESC-CMs after *circALPK2* interference. CCK-8 assay showed that the knockdown of *circALPK2* led to a significant improvement in cardiomyocyte proliferation (Fig. 1J). Meanwhile, we also found a significant increase in the ratio of EdU-positive cells in hESC-CMs subjected to *circALPK2* deletion (Fig. 1K and L). In summary, *circALPK2* has an anti-proliferative effect on human cardiomyocytes.

circALPK2 serves as a *miR-9* sponge in the regulation of cardiomyocyte proliferation

Since circRNAs have the potential to act as miRNA sponges, we used miRcode (<http://www.mircode.org/>) to predict the target miRNAs of *circALPK2*, focusing on 4 candidate targets that have at least 2 binding sites, including *miR-205*, *miR-214*, *miR-24*, and *miR-9* (Fig. 2A). However, RT-qPCR results showed that only *miR-9* was upregulated in hESC-CMs by knockdown of *circALPK2* (Fig. 2B). Therefore, we performed dual luciferase assay to test whether *circALPK2* was able to direct target *miR-9* in HEK293T cells. When either binding site was fused to the luciferase reporter gene downstream of its coding

region, *miR-9* mimics showed a significant inhibitory role in luciferase activity. However, once the binding sites were mutated, *miR-9* mimics failed to inhibit the luciferase activity (Fig. 2C-E). These data indicate that *circALPK2* could act as a sponge for *miR-9*.

To investigate whether *miR-9* is involved in cardiomyocyte proliferation, we performed *miR-9* overexpression in hESC-CMs by transient transfection of *miR-9* mimics (Fig. 2F). *miR-9* overexpression resulted in significantly-decreased expression of *CCNA2* and *CDK1* transcripts in hESC-CMs (Fig. 2G). Consistent with data based on *circALPK2* knockdown, *miR-9* overexpression also led to a significant increase in cardiomyocyte proliferation, as indicated by CCK-8 assay and EdU staining (Fig. 2H-J).

Taken together, the above results demonstrated that *circALPK2* can act as a sponge of *miR-9* to inhibit its expression, and the release of *miR-9* can promote cardiomyocyte proliferation.

The cell cycle-related gene *GSK3B* is a direct target of *miR-9*

To elucidate the mechanisms of *miR-9* in regulation of cardiomyocyte proliferation, we used TargetScan, miRDB and miRTarBase to predict the target genes of *miR-9*, and obtained a list of 80 candidates that were predicted by all three tools (Fig. 3A). Among these candidates, KEGG analysis revealed enrichment of 15 genes in cell growth and death (Fig. 3B), including cell cycle-related gene *GSK3B*, oocyte meiosis-related gene *CPEB4*, as well as other genes involving p53 signaling pathway, apoptosis, ferroptosis, necroptosis and cellular senescence (Fig. 3C). Since both *circALPK2* knockdown and *miR-9* overexpression could stimulate the expression of cell cycle genes and promote cardiomyocyte proliferation (Figs. 1I-L and 2G-J), the target candidates were supposed to be negative regulators of cell cycle and down-regulated by *circALPK2* knockdown. According to RNA-seq data on the control and *circALPK2*-depleted hESC-CMs (Fig. 3C), we attended to investigate whether the cell cycle-related gene *GSK3B* is involved in *circALPK2*/*miR-9*-controlled cell proliferation in hESC-CMs.

RT-qPCR data showed that the expression of *GSK3B* in hESC-CMs was significantly inhibited by both *circALPK2* knockdown and *miR-9* overexpression (Fig. 3D and E), indicating *GSK3B* might be a downstream target of the *circALPK2*/*miR-9* axis. Consistently, the luciferase reporter assay revealed that *miR-9* mimics significantly undermined the activity of luciferase fused with the 3'-UTR of *GSK3B*, which was reversed by mutation of the predicted *miR-9* binding site (Fig. 3F and G). These data indicated that *GSK3B* is a direct target of *miR-9*.

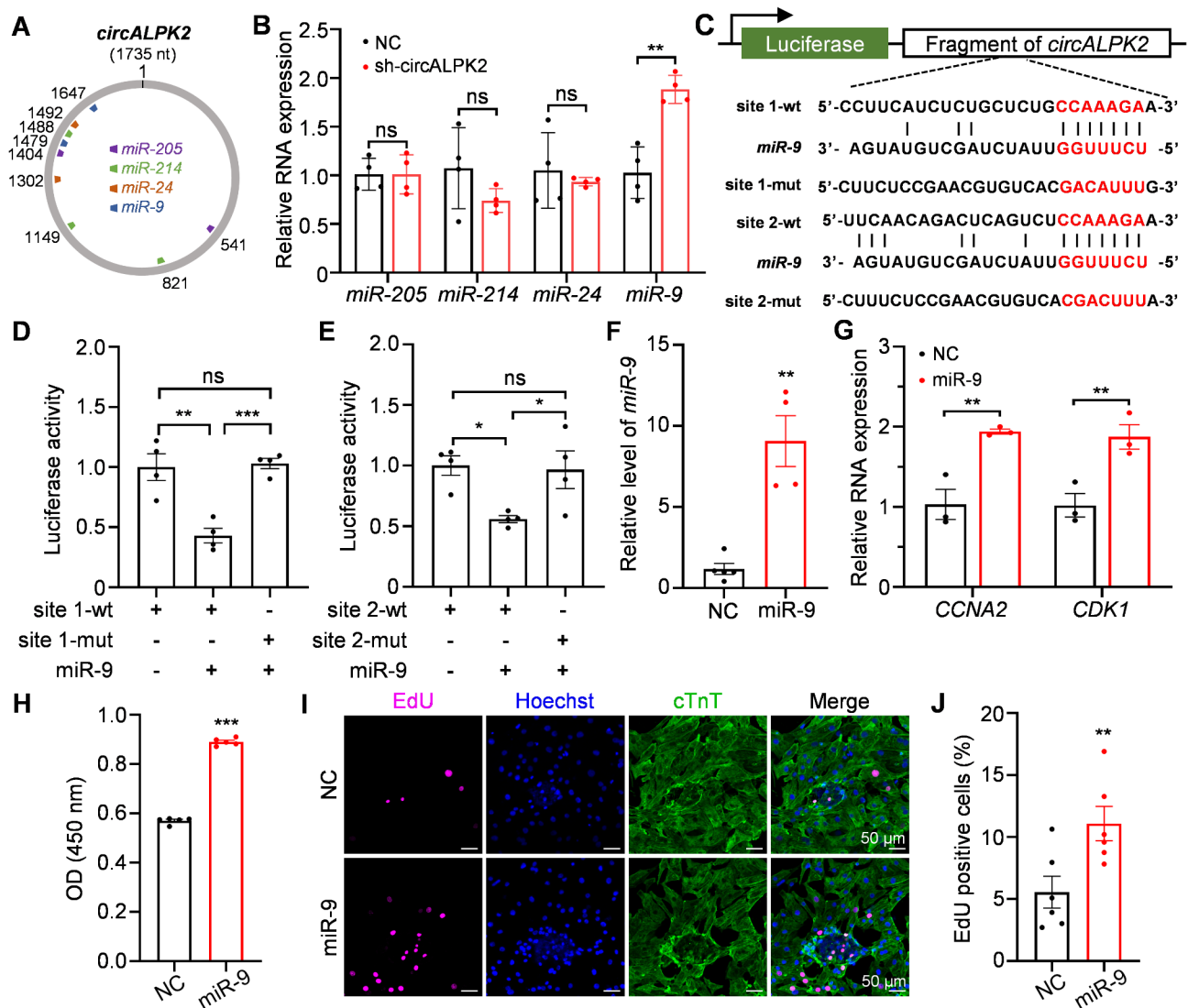


Fig. 2 *miR-9* is a direct target of *circALPK2* in hESC-derived cardiomyocytes. **(A)** Schematic depiction of *circALPK2* showing binding sites of the predicted miRNA targets. **(B)** RT-qPCR detection of miRNAs in hESC-CMs transfected with negative control (NC) and shRNAs specifically targeting *circALPK2* (sh-*circALPK2*) ($n=4$). **(C)** Schematic diagram of luciferase reporter system for the potential binding sites of *miR-9* in *circALPK2*. Two wild-type (wt) *miR-9*-binding regions and their corresponding mutant (mut) fragments were respectively fused with the luciferase gene downstream. **(D-E)** Luciferase analysis showing an inhibitory effect of *miR-9* mimics on the activity of luciferase fused with *circALPK2* fragments carrying wild-type but not mutant *miR-9*-binding regions ($n=4$). **(F-G)** RT-qPCR detection of *miR-9* ($n=4$), *CCNA2* ($n=3$) and *CDK1* ($n=3$) in hESC-CMs transfected with negative control (NC) and *miR-9* mimics. **(H)** CCK-8 assay on cell proliferation (OD 450 nm value) in control and *miR-9*-overexpressed hESC-CMs ($n=5$). **(I)** Immunofluorescence images showing EdU-positive cells (magenta) in hESC-CMs (cTnT-positive, green). Nuclei were stained with Hoechst 33,342 (blue). Scale bar indicates 50 μ m. **(J)** Statistical analysis of the ratio of EdU-positive cells in control and *miR-9*-overexpressed hESC-CMs ($n=6$). Data were shown as mean \pm SEM. One-way ANOVA for multiple comparisons & Student's t-test for comparisons between two groups; * $p < 0.05$, ** $p < 0.01$, *** $p < 0.001$; ns, not significant

GSK3B mediates the *circALPK2*/*miR-9* axis in regulation of cardiomyocyte proliferation

We further determined whether inhibition of the GSK3B protein could promote cardiomyocyte proliferation, the consistent cell phenotype caused by *circALPK2* depletion and *miR-9* overexpression. When compared with the control group, hESC-CMs treated with CHIR, an inhibitor of GSK3B, showed more abundant expression of cell cycle genes *CCNA2* and *CDK1* (Fig. 4A), and a significant increase in cell proliferation activity as indicated by

CCK-8 assay (Fig. 4B) and EdU staining (Fig. 4C and D). Thus, GSK3B is a potential target of the *circALPK2*/*miR-9* axis to regulate cardiomyocyte proliferation.

To determine whether *circALPK2* functions through GSK3B, we performed a rescue experiment in which GSK3B was overexpressed in hESC-CMs with *circALPK2* depletion. Along with the successful overexpression of GSK3B, the expression levels of cell cycle-related genes such as *CCNA2* and *CDK1* were significantly reduced in *circALPK2*-depleted hESC-CMs (Fig. 4E and F).

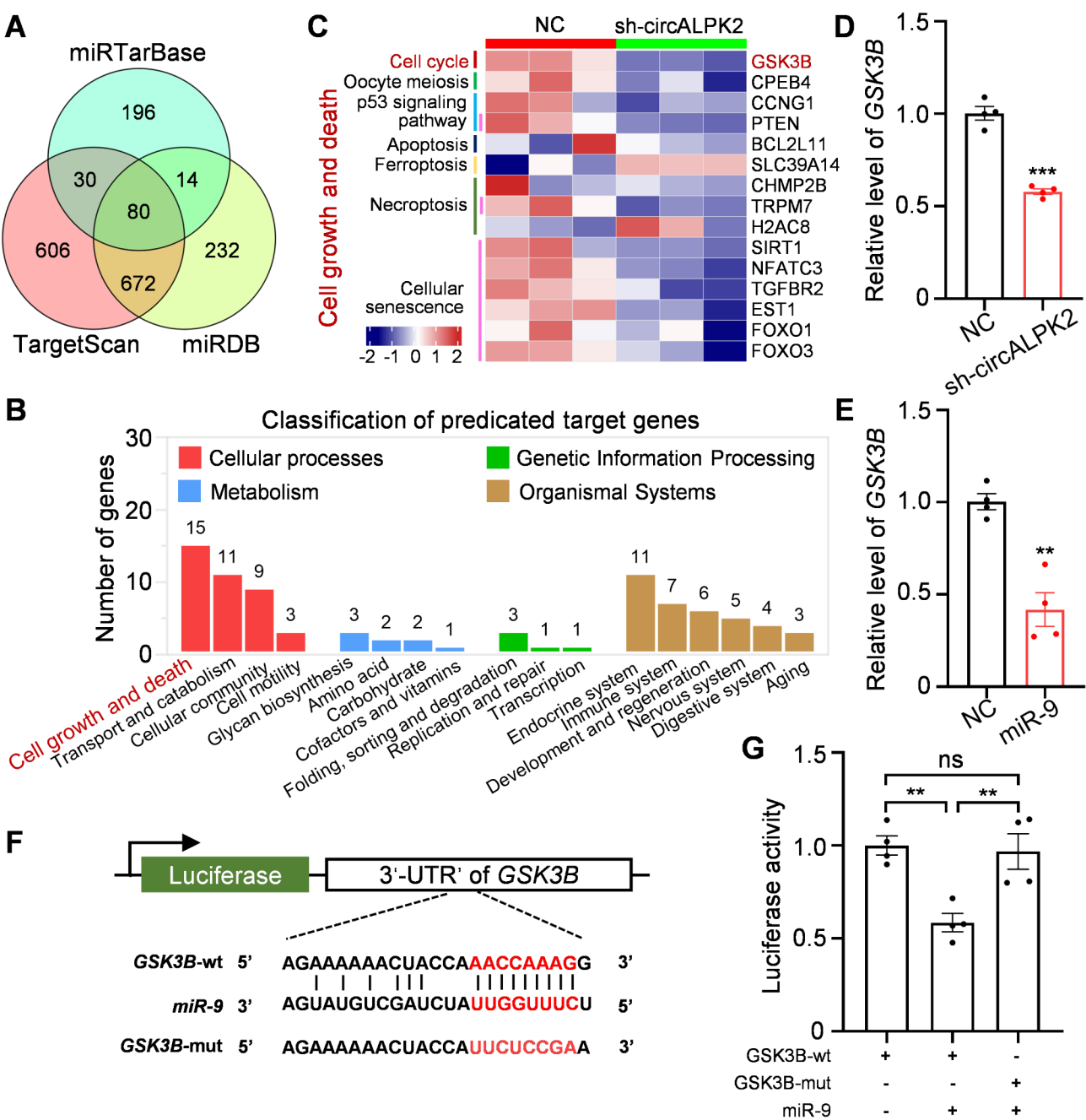


Fig. 3 Identification of *GSK3B* as a direct target of *miR-9*. **(A)** Venn diagram showing 80 overlapped target genes of *miR-9* predicted by three tools, including TargetScan, miRTarBase, and miRDB. **(B)** Bar plot showing Kyoto Encyclopedia of Genes and Genomes (KEGG) pathway classification of the 80 overlapped candidate genes. **(C)** Heatmap showing the gene expression profiles of cell growth and death-related candidate targets of *miR-9* in hESC-CMs transfected with negative control (NC) or shRNAs specifically targeting *circALPK2* (sh-circALPK2), and their subclasses. **(D-E)** RT-qPCR detection of *GSK3B* in the control, *circALPK2*-depleted, and *miR-9*-overexpressed hESC-CMs ($n=4$). **(F)** Schematic diagram of luciferase reporter system carrying the 3'-UTR of *GSK3B* at downstream of the luciferase gene. The potential binding site (wt) of *miR-9* and its mutated target sequence (mut) was shown below. **(G)** Luciferase analysis showing an inhibitory effect of *miR-9* mimics on the activity of luciferase fused with wild-type *GSK3B* 3'-UTR ($n=4$). Data were shown as mean \pm SEM. One-way ANOVA for multiple comparisons & Student's t-test for comparisons between two groups; **, $p < 0.01$, ***, $p < 0.001$; ns, not significant

Meanwhile, the CCK-8 assay showed that *GSK3B* overexpression led to a decrease in cell proliferative capacity in *circALPK2*-depleted hESC-CMs (Fig. 4G). Consistently, the portion of EdU-positive cells was significantly reduced in *circALPK2*-depleted hESC-CMs after *GSK3B* overexpression (Fig. 4H and I). Taken together, the inhibitor of the WNT pathway, *GSK3B*, is a target gene of the *circALPK2*/*miR-9* axis for the regulation of cell proliferation in human cardiomyocytes.

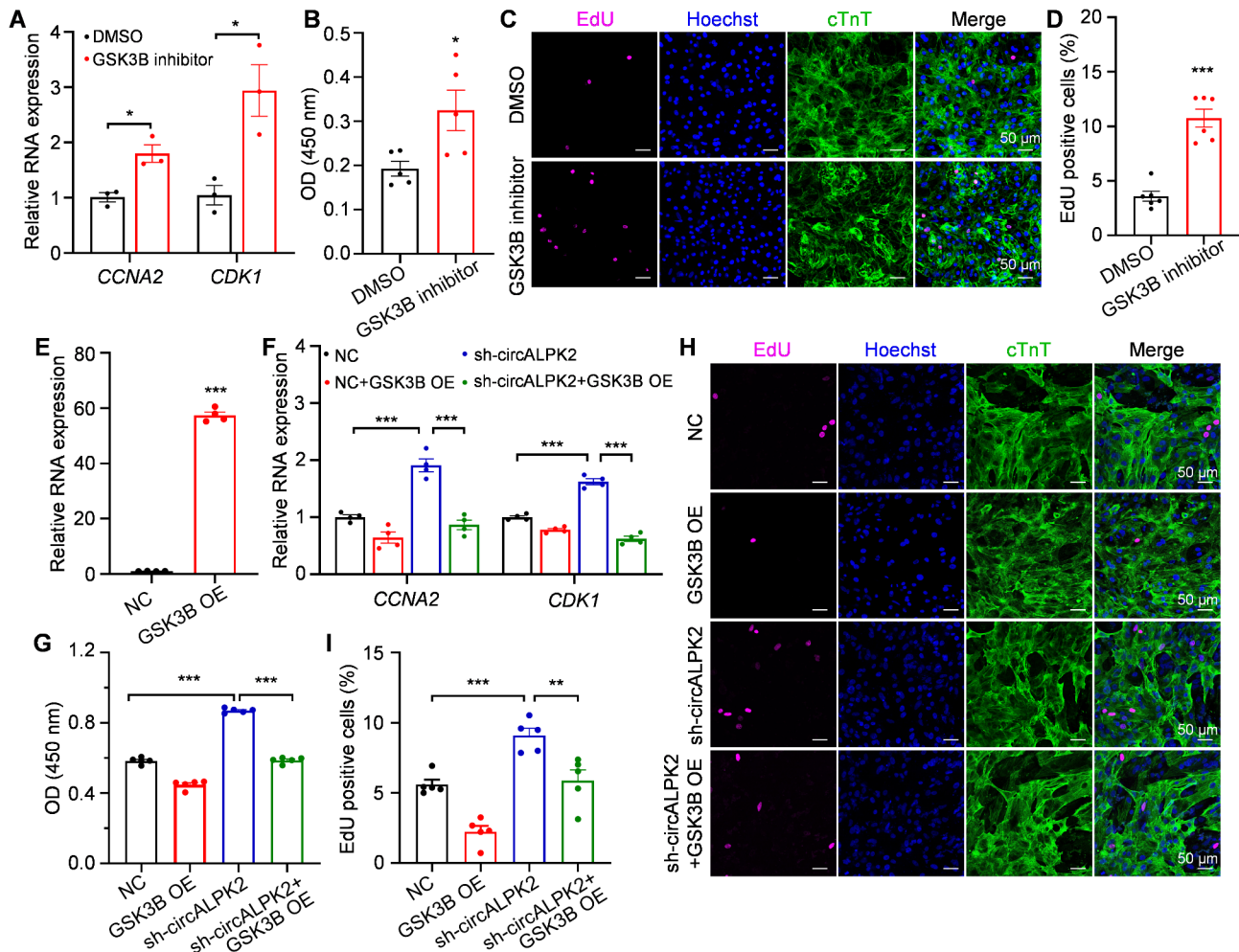


Fig. 4 GSK3B mediates the regulation of *circALPK2* in cardiomyocyte proliferation. **(A)** RT-qPCR detection of cell cycle genes *CCNA2* and *CDK1* in hESC-CMs treated with DMSO and the GSK3B inhibitor CHIR ($n=3$). **(B)** CCK-8 assay on cell proliferation (OD 450 nm value) in DMSO and CHIR-treated hESC-CMs ($n=5$). **(C)** Immunofluorescence images showing EdU-positive cells (magenta) in hESC-CMs (cTnT-positive, green) after DMSO or CHIR treatment. Nuclei were stained with Hoechst 33,342 (blue). Scale bar indicates 50 μ m. **(D)** Statistical analysis of the ratio of EdU-positive cells in control and CHIR-treated hESC-CMs ($n=6$). **(E)** RT-qPCR data showing successful overexpression of *GSK3B* in hESC-CMs (GSK3B OE) ($n=4$). NC indicates negative control. The transfection efficiency of lentiviral overexpression vectors is presented in Supplementary Figure S3. **(F)** RT-qPCR detection of cell cycle genes *CCNA2* and *CDK1* in hESC-CMs subjected to shRNA-mediated *circALPK2* depletion (sh-*circALPK2*) with/without GSK3B overexpression ($n=4$). **(G-I)** Data from CCK-8 (G) and EdU staining (magenta) assays (H-I) showing cell proliferative capacity of wild-type hESC-CMs and *circALPK2*-depleted hESC-CMs with/without GSK3B overexpression ($n=5$). Data were shown as mean \pm SEM. One-way ANOVA for multiple comparisons & Student's t-test for comparisons between two groups; * $p < 0.05$, ** $p < 0.01$, *** $p < 0.001$; ns, not significant

Knockdown of *circALPK2* enhances the cardiac repair capacity of hESC-CMs

We evaluated the cardiac repair capacity of wild-type and *circALPK2*-depleted hESC-CMs following intramyocardial injection into the SCID/beige mice subjected to MI ($n=7$ for each group). Echocardiographic analysis was performed at both day 14 (Supplementary Fig. S4) and day 28 (Fig. 5A-C) post-MI and cell transplantation. While MI surgery resulted in a significant impairment of systolic heart function, as indicated by a marked decrease in left ventricular EF and FS, the injection of either wild-type or *circALPK2*-depleted hESC-CMs noticeably improved the cardiac function of MI mice (Fig. 5B and C,

Supplementary Fig. S4). Notably, the knockdown of *circALPK2* in hESC-CMs significantly elevated the EF and FS values in hESC-CM-injected MI mice (Fig. 5B and C, Supplementary Fig. S4).

At day 28 post-MI, the relative area of infarction was assessed using Masson's trichrome staining on heart tissue sections adjacent to the LAD ligation sites. Consistent with the echocardiographic data, the relative infarct area was smaller in mice that received *circALPK2*-depleted hESC-CM injections compared to those that received wild-type hESC-CM injections (Fig. 5D and E). These findings were further corroborated by the expression of

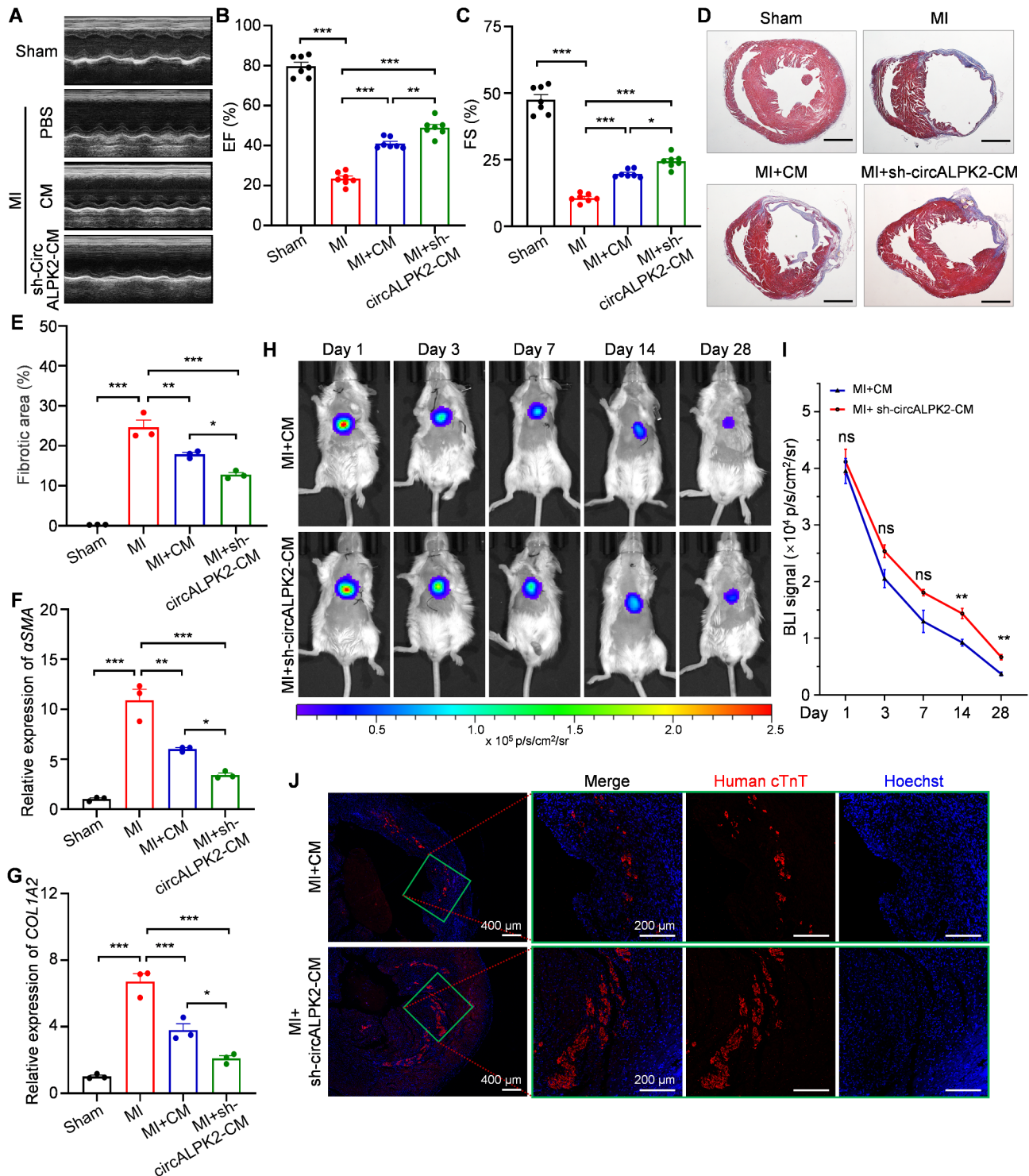


Fig. 5 *CircALPK2* depletion enhances the cardiac repair capacity of hESC-CMs. **(A)** Representative echocardiogram of mice at day 28 in the Sham-operated control group (Sham), the myocardial infarction group (MI), the MI plus wild-type hESC-CM injection group (MI + CM), and the MI plus circALPK2-knockdown hESC-CM injection group (MI + sh-circALPK2-CM). **(B-C)** Quantitative analysis of left ventricular ejection fraction (EF) and fractional shortening (FS) in mice at day 28 post-MI ($n = 7$). **(D)** Representative Masson's trichrome staining images of heart tissue sections in different groups. Scale bar indicates 1 mm. **(E)** Statistical analysis of relative fibrosis area from Masson's trichrome staining images ($n = 3$). **(F-G)** RT-qPCR detection of fibrotic markers α SMA and COL1A2 in mouse hearts from different groups ($n = 3$). **(H)** Representative in vivo bioluminescence images (BLI) of mice at the indicated days post-cell transplantation. **(I)** Quantitative analysis of BLI signals at different groups ($n = 3$). **(J)** Immunofluorescence images showing hESC-CM retention (human-specific cTnT-positive, red) in mouse hearts at day 7 post-cell transplantation. Nuclei were stained with Hoechst 33,342 (blue). Data were shown as mean \pm SEM. One-way ANOVA for multiple comparisons & Student's t-test for comparisons between two groups; * $p < 0.05$, ** $p < 0.01$, *** $p < 0.001$

fibrotic markers, including α SMA and COL1A2 (Fig. 5F and G).

To evaluate the retention of injected cells, we performed BLI in MI mice that received hESC-CMs engineered with a luciferase reporter, following transfection with either control or *circALPK2* shRNA. Although BLI signals gradually diminished from day 1 to day 28 post-cell transplantation, they remained detectable in the hearts of mice in both groups (Fig. 5H). Notably, *circALPK2* knockdown in hESC-CMs enhanced cell retention in the MI mouse hearts from day 3 onwards, as evidenced by stronger BLI signals in the *circALPK2* knockdown group compared to the control group, with statistical significance at both day 14 and day 28 (Fig. 5H and I). Immunofluorescence staining, using an antibody specific to human but not mouse cTnT, was also performed on heart sections at day 7 post-transplantation. These results further confirmed the enhanced retention of hESC-CMs in MI heart in the *circALPK2* knockdown group compared to the wild-type cell injections (Fig. 5J).

Therefore, our data indicate that *circALPK2* and its downstream targets may represent novel therapeutic targets for enhancing the retention of engrafted cells and improving the cardiac repair potential of hESC-CMs.

Discussion

Exploring the mechanisms controlling human cardiomyocyte proliferation has emerged as one of the most promising approaches for developing effective therapies for CVDs via activating endogenous regeneration of cardiomyocytes or enhancing the survival and engraftment rate of transplanted PSC-derived cardiomyocytes [22–24]. Previous studies have revealed the involvement of circRNAs in the physiology and pathology of CVDs, but their roles in human cardiomyocyte proliferation are still unknown [13, 17, 25–28]. In the current study, we harnessed hESC-CMs to decipher circRNA functions in human cardiomyocyte proliferation and identified *circALPK2* as a negative regulator of cardiomyocyte proliferation and cardiac regeneration. We further reveal that *circALPK2* can act as a *miR-9* sponge to relieve its repressive effect on *GSK3B*, while the inhibition of *GSK3B* protein promoted cardiomyocyte proliferation.

Our study indicates that the cardiomyocyte-enriched *circALPK2* arises from the back-splicing of the 4th exon of its host gene *ALPK2*. *ALPK2* depletion has been shown to impair both zebrafish heart development and cardiomyocyte differentiation from hESCs, but displays no overt cardiac phenotype in mice [18, 19]. When exploring the observed discrepancy between human and mouse models, the participation of *circALPK2* may also need to be considered, in addition to the evolutionary differences of the *ALPK2* protein. While the *ALPK2* protein was shown to promote transitioning from mesoderm toward

the cardiomyocyte lineage during cardiac differentiation [18], we first demonstrated that *circALPK2* inhibited cell proliferation and cardiac repair capacity of the differentiated cardiomyocytes. These evidences indicate that the *ALPK2* gene cluster might play multiple roles during cardiac development and cardiac regeneration.

Interestingly, the *ALPK2* protein and *circALPK2* displayed similar regulatory effects on WNT signaling, a multiphasic regulator of cardiac development [29, 30]. At the earliest stages of cardiac development, *ALPK2* acts as a repressor of WNT signaling to promote cardiomyocyte differentiation in both zebrafish and humans, although the detailed mechanism is still implicit [18]. In our study, we found that *GSK3B*, a negative regulator of WNT signaling, was positively regulated by *circALPK2*. Meanwhile, our data and previous results showed that *GSK3B* inhibitor CHIR could promote the proliferation of both hESC- and hiPSC-derived cardiomyocytes [30], while *GSK3B* overexpression could impede the *circALPK2* depletion-induced cardiomyocyte proliferation. Thus, we believe that the *ALPK2* gene cluster plays critical regulatory roles in human cardiac development and regeneration through the coordinated regulation of the WNT signaling pathway by both *ALPK2* protein and *circALPK2*.

Mechanistically, we identified *miR-9* as a direct intermediary between *circALPK2* and *GSK3B*. Although *miR-9* has emerged as a versatile regulator of neurogenesis, human brain pathologies, and cancers, its role in cardiac development is largely unknown [31, 32]. In this study, we found that *miR-9* mimics significantly promoted cell proliferation in hESC-CMs, extending the functional list of *miR-9*. Notably, *miR-9* was shown to bind to both *circALPK2* and *GSK3B* mRNA directly. The binding of *miR-9* to *circALPK2* will result in a downstream increase of *GSK3B*, ultimately leading to the inhibition of WNT activation. Our study revealed a critical role of the *circALPK2/miR-9/GSK3B* axis in the regulation of cardiomyocyte proliferation and cardiac regeneration.

One limitation of this study should be considered when interpreting our results. The hPSC-derived cardiomyocytes represent immature cardiomyocytes at embryonic or fetal stages, which maintain the proliferative capacity [33]. Although the *circALPK2/miR-9/GSK3B* axis was shown to control cardiomyocyte proliferation and the cardiac repair ability of hESC-CMs, additional studies are required to investigate its regulatory effect on cardiac proliferation and regeneration at the adult stage.

Conclusions

We demonstrated a negative regulatory role of *circALPK2* in human cardiomyocyte proliferation via the *circALPK2/miR-9/GSK3B* axis, which may serve as a new

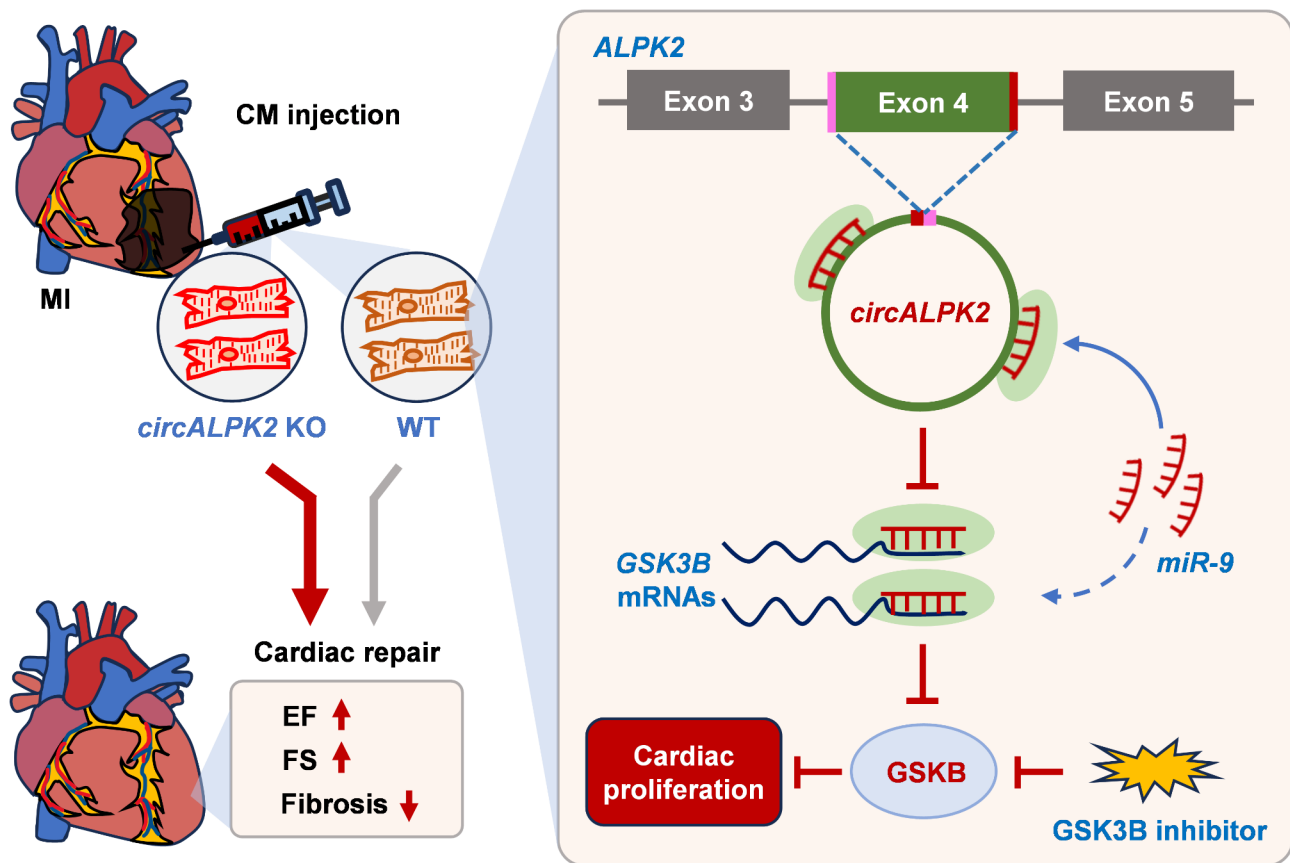


Fig. 6 *CircALPK2* regulates human cardiomyocyte proliferation via the miR-9/GSK3B axis. *CircALPK2* inhibits human cardiomyocyte (CM) proliferation by sponging *miR-9* and releasing *miR-9* from *GSK3B* mRNA, ultimately leading to increased expression of *GSK3B* protein and inhibition of the WNT signaling pathway. *CircALPK2* knockout (KO) enhances the therapeutic potential of hPSC-CMs in treating myocardial infarction (MI). WT: wild-type; EF: ejection fraction; FS: fractional shortening

target for the massive expansion of hPSC-CMs and promotion of cardiac regeneration (Fig. 6).

Abbreviations

ALPK2	Alpha protein kinase 2
circALPK2	circRNA ALPK2
circRNAs	circular RNAs
CVDs	cardiovascular diseases
EF	ejection fraction
FS	fraction of shortening
GSK3B	glycogen synthase kinase 3β
hESC-CMs	human embryonic stem cell-derived cardiomyocytes
hPSC-CMs	human pluripotent stem cell-derived cardiomyocytes
MI	myocardial infarction
miRNA	microRNA

Supplementary Information

The online version contains supplementary material available at <https://doi.org/10.1186/s13287-025-04230-8>.

Supplementary Material 1

Supplementary Material 2

Acknowledgements

The authors declare that they have not use AI-generated work in this manuscript.

Authors' contributions

W.L., S.H., M.Y., and J.T. supervised the entire project. H.W., X.J., and H.F. performed most of the experiments and analyzed the data. H.F., J.L., Y.L. (Li), Y.L. (Lin), D.Z., and X.H. performed in vivo studies. H.W., X.J., W.L., and S.H. wrote and revised the manuscript.

Funding

This work was funded by the National Key R&D Program of China (2022YFA1104300, 2021YFA1101902), National Natural Science Foundation of China (82241202, 82170364, 81970223), Natural Science Foundation of Jiangsu Province (BK20240001), Open Project of Hubei Key Laboratory of Embryonic Stem Cell Research (ESOF2023008), Jiangsu Cardiovascular Medicine Innovation Center (CXZX202210), National Center for International Research (2017B01012), and A Project Funded by the Priority Academic Program Development of Jiangsu Higher Education Institutions.

Data availability

The data supporting the findings of this study are available within the article and its supplementary materials. The raw sequence data reported in this paper have been deposited in the Genome Sequence Archive (Genomics, Proteomics & Bioinformatics 2021) in National Genomics Data Center (Nucleic Acids Res 2022), China National Center for Bioinformation / Beijing Institute of Genomics, Chinese Academy of Sciences (GSA-Human: HRA008797) that are publicly accessible at <https://ngdc.cncb.ac.cn/gsa-human>.

Declarations

Ethics approval and consent to participate

Experiments involving human cells and animals were approved by the Ethics Committee of First Affiliated Hospital of Soochow University (No. 2022—519; Project title: Effects of noncoding RNAs on the maturation and therapeutic potential of hPSC-derived cardiac cells in cardiovascular diseases; Date of approval: March 1, 2022). Human cardiac cells used in this study were differentiated in vitro from H1 hESCs, a human ESC line established following ethical approval and informed consent [20].

Consent for publication

Not applicable.

Competing interests

The authors declare that they have no conflict of interest.

Author details

¹Department of Cardiovascular Surgery of the First Affiliated Hospital & Institute for Cardiovascular Science, Collaborative Innovation Center of Hematology, State Key Laboratory of Radiation Medicine and Protection, Suzhou Medical College, Soochow University, Suzhou 215000, Jiangsu, China

²Hubei Key Laboratory of Embryonic Stem Cell Research, School of Basic Medicine Science, Hubei University of Medicine, Shiyan 442000, Hubei, China

Received: 26 September 2024 / Accepted: 14 February 2025

Published online: 01 March 2025

References

1. Tsao CW, Aday AW, Almarazooq ZI, Anderson CAM, Arora P, Avery CL, et al. Heart Disease and Stroke Statistics-2023 update: a Report from the American Heart Association. *Circulation*. 2023;147(8):e93–621.
2. Salerno N, Salerno L, Marino F, Scalise M, Chieffalo A, Panuccio G, et al. Myocardial regeneration protocols towards the routine clinical scenario: an unseemly path from bench to bedside. *EClinicalMedicine*. 2022;50:101530.
3. Secco I, Giacca M. Regulation of endogenous cardiomyocyte proliferation: the known unknowns. *J Mol Cell Cardiol*. 2023;179:80–9.
4. Li Y, Feng J, Song S, Li H, Yang H, Zhou B, et al. gp130 controls cardiomyocyte proliferation and heart regeneration. *Circulation*. 2020;142(10):967–82.
5. Du J, Zheng L, Gao P, Yang H, Yang WJ, Guo F, et al. A small-molecule cocktail promotes mammalian cardiomyocyte proliferation and heart regeneration. *Cell Stem Cell*. 2022;29(4):545–58. e13.
6. Oikonomopoulos A, Kitani T, Wu JC. Pluripotent stem cell-derived cardiomyocytes as a platform for cell therapy applications: Progress and hurdles for clinical translation. *Mol Ther*. 2018;26(7):1624–34.
7. Abbas N, Perbellini F, Thum T. Non-coding RNAs: emerging players in cardiomyocyte proliferation and cardiac regeneration. *Basic Res Cardiol*. 2020;115(5):52.
8. Wang B, Xu M, Li M, Wu F, Hu S, Chen X, et al. miR-25 promotes Cardiomyocyte Proliferation by Targeting FBXW7. *Mol Ther Nucleic Acids*. 2020;19:1299–308.
9. Eulalio A, Mano M, Dal Ferro M, Zentilin L, Sinagra G, Zacchigna S, et al. Functional screening identifies miRNAs inducing cardiac regeneration. *Nature*. 2012;492(7429):376–81.
10. Liang D, Li J, Wu Y, Zhen L, Li C, Qi M, et al. miRNA-204 drives cardiomyocyte proliferation via targeting Jarid2. *Int J Cardiol*. 2015;201:38–48.
11. Arif M, Pandey R, Alam P, Jiang S, Sadayappan S, Paul A, et al. MicroRNA-210-mediated proliferation, survival, and angiogenesis promote cardiac repair post myocardial infarction in rodents. *J Mol Med (Berl)*. 2017;95(12):1369–85.
12. Renikunta HV, Lazarow K, Gong Y, Shukla PC, Nageswaran V, Giral H, et al. Large-scale microRNA functional high-throughput screening identifies miR-515-3p and miR-519e-3p as inducers of human cardiomyocyte proliferation. *iScience*. 2023;26(5):106593.
13. Huang S, Li X, Zheng H, Si X, Li B, Wei G, et al. Loss of Super-enhancer-regulated circRNA Nfix induces Cardiac Regeneration after myocardial infarction in adult mice. *Circulation*. 2019;139(25):2857–76.
14. Zhu Y, Zhao P, Sun L, Lu Y, Zhu W, Zhang J, et al. Overexpression of circRNA SNRK targets mir-103-3p to reduce apoptosis and promote cardiac repair through GSK3beta/beta-catenin pathway in rats with myocardial infarction. *Cell Death Discov*. 2021;7(1):84.
15. Si X, Zheng H, Wei G, Li M, Li W, Wang H, et al. circRNA Hipk3 induces Cardiac Regeneration after myocardial infarction in mice by binding to Notch1 and miR-133a. *Mol Ther Nucleic Acids*. 2020;21:636–55.
16. Hunkler HJ, Gross S, Thum T, Bar C. Non-coding RNAs: key regulators of reprogramming, pluripotency, and cardiac cell specification with therapeutic perspective for heart regeneration. *Cardiovasc Res*. 2022;118(15):3071–84.
17. Lei W, Feng T, Fang X, Yu Y, Yang J, Zhao ZA, et al. Signature of circular RNAs in human induced pluripotent stem cells and derived cardiomyocytes. *Stem Cell Res Ther*. 2018;9(1):56.
18. Hofsteen P, Robitaille AM, Strash N, Palpant N, Moon RT, Pabon L, et al. ALPK2 promotes Cardiogenesis in zebrafish and human pluripotent stem cells. *iScience*. 2018;2:88–100.
19. Bogomolovas J, Feng W, Yu MD, Huang S, Zhang L, Trexler C, et al. Atypical ALPK2 kinase is not essential for cardiac development and function. *Am J Physiol Heart Circ Physiol*. 2020;318(6):H1509–15.
20. Thomson JA, Itskovitz-Eldor J, Shapiro SS, Waknitz MA, Swiergiel JJ, Marshall VS, et al. Embryonic stem cell lines derived from human blastocysts. *Science*. 1998;282(5391):1145–7.
21. Han X, Qu L, Yu M, Ye L, Shi L, Ye G, et al. Thiamine-modified metabolic reprogramming of human pluripotent stem cell-derived cardiomyocyte under space microgravity. *Signal Transduct Target Ther*. 2024;9(1):86.
22. Guo QY, Yang JQ, Feng XX, Zhou YJ. Regeneration of the heart: from molecular mechanisms to clinical therapeutics. *Mil Med Res*. 2023;10(1):18.
23. Zhang J, Bolli R, Garry DJ, Marban E, Menasche P, Zimmermann WH, et al. Basic and Translational Research in Cardiac Repair and Regeneration: JACC State-of-the-art review. *J Am Coll Cardiol*. 2021;78(21):2092–105.
24. Hashimoto H, Olson EN, Bassel-Duby R. Therapeutic approaches for cardiac regeneration and repair. *Nat Rev Cardiol*. 2018;15(10):585–600.
25. Zeng Z, Xia L, Fan S, Zheng J, Qin J, Fan X, et al. Circular RNA CircMAP3K5 acts as a MicroRNA-22-3p sponge to Promote Resolution of Intimal Hyperplasia Via TET2-Mediated smooth muscle cell differentiation. *Circulation*. 2021;143(4):354–71.
26. Li H, Xu JD, Fang XH, Zhu JN, Yang J, Pan R, et al. Circular RNA circRNA_000203 aggravates cardiac hypertrophy via suppressing miR-26b-5p and miR-140-3p binding to Gata4. *Cardiovasc Res*. 2020;116(7):1323–34.
27. Zheng H, Huang S, Wei G, Sun Y, Li C, Si X, et al. CircRNA Samd4 induces cardiac repair after myocardial infarction by blocking mitochondria-derived ROS output. *Mol Ther*. 2022;30(11):3477–98.
28. Gao XQ, Liu CY, Zhang YH, Wang YH, Zhou LY, Li XM, et al. The circRNA CNEACR regulates necroptosis of cardiomyocytes through Foxa2 suppression. *Cell Death Differ*. 2022;29(3):527–39.
29. Ueno S, Weidinger G, Osugi T, Kohn AD, Golob JL, Pabon L, et al. Biphasic role for Wnt/beta-catenin signaling in cardiac specification in zebrafish and embryonic stem cells. *Proc Natl Acad Sci U S A*. 2007;104(23):9685–90.
30. Buikema JW, Lee S, Goodyer WR, Maas RG, Chirikian O, Li G, et al. Wnt activation and reduced cell-cell contact synergistically induce massive expansion of functional human iPSC-Derived cardiomyocytes. *Cell Stem Cell*. 2020;27(1):50–63. e5.
31. Coolen M, Katz S, Bally-Cuif L. miR-9: a versatile regulator of neurogenesis. *Front Cell Neurosci*. 2013;7:220.
32. Li X, Zeng Z, Wang J, Wu Y, Chen W, Zheng L, et al. MicroRNA-9 and breast cancer. *Biomed Pharmacother*. 2020;122:109687.
33. Singh BN, Yucel D, Garay BI, Tolkacheva EG, Kyba M, Perlingeiro RCR, et al. Proliferation and maturation: Janus and the art of Cardiac tissue Engineering. *Circ Res*. 2023;132(4):519–40.

Publisher's note

Springer Nature remains neutral with regard to jurisdictional claims in published maps and institutional affiliations.